### Title

In-Reservoir Physical Processes Modulate Aqueous and Biological Methylmercury Export from a Seasonally Anoxic Reservoir




### Journal

Environmental Science and Technology, 56(19)

### ISSN

0013-936X



### Authors

Baldwin, Austin K
Eagles-Smith, Collin A
Willacker, James J
et al.



### Publication Date

2022-10-04

### DOI

10.1021/acs.est.2c03958

Peer reviewed

Environmental Science & Technology

pubs.acs.org/est

Article

# In-Reservoir Physical Processes Modulate Aqueous and Biological Methylmercury Export from a Seasonally Anoxic Reservoir

Austin K. Baldwin,* Collin A. Eagles-Smith, James J. Willacker, Brett A. Poulin, David P. Krabbenhoft, Jesse Naymik, Michael T. Tate, Dain Bates, Nick Gastelecutto, Charles Hoovestol, Chris Larsen, Alysa M. Yoder, James Chandler, and Ralph Myers

Cite This: *Environ. Sci. Technol.* 2022, 56, 13751−13760

Read Online

ACCESS | Metrics & More | Article Recommendations | Supporting Information

**ABSTRACT:** Anoxic conditions within reservoirs related to thermal stratification and oxygen depletion lead to methylmercury (MeHg) production, a key process governing the uptake of mercury in aquatic food webs. Once formed within a reservoir, the timing and magnitude of the biological uptake of MeHg and the relative importance of MeHg export in water versus biological compartments remain poorly understood. We examined the relations between the reservoir stratification state, anoxia, and the concentrations and export loads of MeHg in aqueous and biological compartments at the outflow locations of two reservoirs of the Hells Canyon Complex (Snake River, Idaho-Oregon). Results show that (1) MeHg concentrations in filter-passing water, zooplankton, suspended particles, and detritus increased in response to reservoir destratification; (2) zooplankton MeHg strongly correlated with MeHg in filter-passing water during destratification; (3) reservoir anoxia appeared to be a key control on MeHg export; and (4) biological MeHg, primarily in zooplankton, accounted for only 5% of total MeHg export from the reservoirs (the remainder being aqueous compartments). These results improve our understanding of the role of biological incorporation of MeHg and the subsequent downstream release from seasonally stratified reservoirs and demonstrate that in-reservoir physical processes strongly influence MeHg incorporation at the base of the aquatic food web.

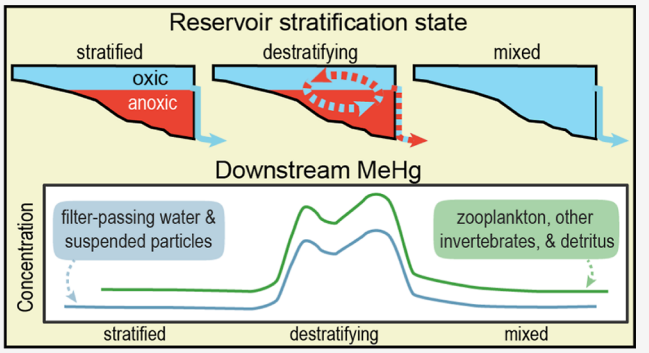


**KEYWORDS:** *zooplankton, suspended sediment, destratification, biological uptake, bioaccumulation, aquatic food web, methylation, anoxia*

## INTRODUCTION

Reservoirs are critical infrastructure in both developed and developing nations, comprising a global surface area roughly equivalent to that of natural lakes[1] and providing renewable energy, water storage, flood control, and other services. Global construction of reservoirs is expected to increase in the coming decades to meet the water supply and renewable energy needs of a growing and economically developing human population.[2] However, while the socioeconomic benefits of reservoirs are clear, reservoirs also dramatically alter natural flows and the ecosystem structure.[3,4]

Seasonal anoxia from decomposing organic matter is common in reservoirs around the world and is expected to increase with climate and land-use change.[5−8] Anoxia is a key driver of (MeHg) production and increased concentrations in metalimnion and hypolimnion.[9] Upon seasonal thermal destratification (i.e., mixing), MeHg stored in anoxic waters at depth may become available for biological uptake.[10,11] MeHg is incorporated into the food web via bioconcentration by phytoplankton and subsequent biomagnification in higher trophic levels,[12] which can result in a >1 million-fold increase in MeHg levels from water to top predator fish.[13] As a potent neurotoxin and endocrine disruptor, MeHg causes adverse health effects in both wildlife and humans.[14−16] Consequently, MeHg contamination is the leading reason for issuing fish consumption advisories in the United States.[13]

Although MeHg produced and retained in reservoirs can influence in-reservoir biological exposure, and destratification mobilizes those stored pools of MeHg for downstream export,[10,17−19] the timing and relative magnitude and contributions of MeHg export in aqueous versus biological compartments remain poorly understood. This is an important information gap because of its implications on MeHg uptake by

Received: June 1, 2022
Revised: September 1, 2022
Accepted: September 7, 2022
Published: September 15, 2022

downstream biota because fish primarily assimilate MeHg through their diet rather than through aqueous exposure.[20,21]

We examined the downstream export of MeHg in aqueous (filter-passing and particulate) and biological compartments (zooplankton, other invertebrates, fish, and coarse and fine detritus) from two reservoirs in the Hells Canyon Complex (HCC) along the Snake River (USA) over a 16-month period. We relate the outflow aqueous and biological MeHg concentrations to the reservoir stratification status and anoxic volume. We also compare the MeHg export loads in aqueous and biological compartments to understand the relative importance of each compartment in transferring MeHg downstream. Our findings improve the understanding of how in-reservoir physical processes influence MeHg incorporation into reservoir food webs and its subsequent export to downstream habitats.

## METHODS

**Study Area.** The HCC comprises three successive reservoirs on the Snake River along the Idaho-Oregon border (USA). Brownlee Reservoir is the most upstream and largest of the reservoirs (Figure S1) and flows into Oxbow Reservoir, which in turn flows into Hells Canyon Reservoir. During summer months, much of Brownlee Reservoir thermally stratifies and becomes anoxic in portions of the transition zone, metalimnion, and throughout the hypolimnion.[17,22] During late summer and fall, cool, inflowing water gradually erodes the thermal stratification, mixing the anoxic waters with the overlying oxic waters. This process, referred to hereafter as destratification, occurs slowly over the course of several months (August to December), after which the reservoir is thermally mixed and oxic and remains so throughout the winter and early spring.[17] The forebay of the downstream Hells Canyon Reservoir also typically stratifies during summer, whereas stratification is limited and inconsistent in Oxbow Reservoir.[22]

The Snake River through the HCC is listed as impaired for mercury by the States of Idaho and Oregon. Reservoir stratification is an important driver of Hg cycling in the HCC.[17,23] During stratification periods, aqueous methylmercury concentrations are elevated in the anoxic and hypoxic areas of the transition zone, metalimnion, and hypolimnion, relative to the epilimnion. This contrasts with nonstratified (well-mixed) periods when concentrations are vertically uniform and substantially lower.[23] Additionally, the destratification period (August to December) coincides with the elevated MeHg concentrations in water samples at the reservoir outflows, suggesting that some portion of the metalimnetic and hypolimnetic MeHg is exported downstream.[17]

**Sample Collection.** To quantify the role of reservoir physical processes on the downstream export of aqueous and biological MeHg, we collected aqueous and biological samples every 2 weeks between June 2018 and September 2019 at the dam outflows of Brownlee and Oxbow Reservoirs (Figure S1). Aqueous samples collected at the Brownlee Inflow during the same period are also included for comparison with the Brownlee Outflow. Additionally, to provide greater temporal and spatial context for the results presented, aqueous mercury concentrations and loads over a broader period (June 2014 to March 2021), and from two additional sites (near Melba, Idaho, 102 River Miles upstream of Brownlee Inflow and above the confluences of five major tributaries; and at the dam outflow of Hells Canyon Reservoir, the lowermost reservoir in the HCC), are available online (concentrations)[24] and included in the Supporting Information (concentrations and loads).[24] Biological samples were limited to Brownlee Outflow and Oxbow Outflow for logistical, safety, and (or) permitting reasons and, in the case of the Melba and Brownlee Inflow sites, because fish can travel both upstream and downstream, complicating load estimations. The biological sample concentrations are available online.[25]

**Water Samples.** Water sample collection, processing, and analytical methods are described elsewhere.[17,24] Briefly, water samples were collected using depth-integrated and grab methods, depending on the access at different locations. Within 24 h of collection, water samples were filtered through a 0.7 $\mu$m pore size quartz fiber filter (QFF; precombusted to 550 °C). Particulate samples, which contained inorganic particles and particulate organic carbon with some minor contributions of phytoplankton and zooplankton,[24] were frozen (−20 °C) in the dark; filter-passing fractions were stored in Teflon bottles and acidified to 1% volume-to-volume with ultraclean hydrochloric acid. Samples were analyzed by the U.S. Geological Survey (USGS) Mercury Research Laboratory (MRL; Madison, Wisconsin, USA) for filter-passing THg and MeHg ($THg_F$ and $MeHg_F$), particulate volumetric THg and MeHg ($THg_{PV}$ and $MeHg_{PV}$), and suspended particulate material (SPM). $THg_F$ and $THg_{PV}$ analyses followed USEPA Method 1631, Revision E,[26] with modifications by the MRL.[27] $MeHg_F$ and $MeHg_{PV}$ analyses followed USEPA Method 1630,[28] with modifications by the MRL.[29] SPM was collected on a preweighed QFF that was lyophilized and weighed to determine the mass of particulates collected in comparison to the volume of water filtered. Particulate gravimetric MeHg ($MeHg_{PG}$, in ng/g) was calculated from the concentrations of $MeHg_{PV}$ (ng/L) and SPM. The results of the water sample field blanks and field duplicates are summarized in Figure S2 and Table S1, respectively.

**Biological Samples.** Biological samples were collected from the same reservoir outflow locations as the aqueous samples and typically within 5 days of aqueous sampling. During each sampling event, biological samples were collected with a custom 1.5 × 0.9 m (1.39 $m^2$ sampling area) net with 5 mm mesh to capture fish and coarse materials and a 30 cm diameter (0.07 $m^2$ sampling area) Wisconsin-style plankton net with 125 $\mu$m mesh used to capture plankton and other fine materials. The fish net was designed to capture drifting, juvenile fish that had passed through the dam turbines, rather than large fish which generally avoid the turbine intakes. Floats attached to the nets ensured consistent sampling depth near the water surface. At each site, the nets were deployed in the main flowline for either 15−36 min (coarse net; median 31 min) or 3−21 min (plankton net; median 6 min) per sample depending on the flows, which were quantified with a flow meter installed on the sampling nets. The turbulence of flow below the dams kept the water column well mixed at the sampling locations. Two or three replicate samples were collected from each net per sampling event and site. All biological samples were kept on ice in a cooler while in the field (up to 6 h) and then frozen (−20 °C) until further processing.

In the laboratory, the samples were thawed and quantitatively split using either a Canton tray (coarse net samples) or a Folsom splitter (plankton net samples) to a density that could be effectively sorted and then sorted into five classes: fish, zooplankton, other invertebrates (i.e., terrestrial and benthic invertebrates), coarse (≥5 mm) detritus, and fine (≤5 mm) detritus. All samples were oven-dried to a constant mass and weighed to either 0.001 g (large pieces of coarse detritus) or


https://doi.org/10.1021/acs.est.2c03958
Environ. Sci. Technol. 2022, 56, 13751−13760

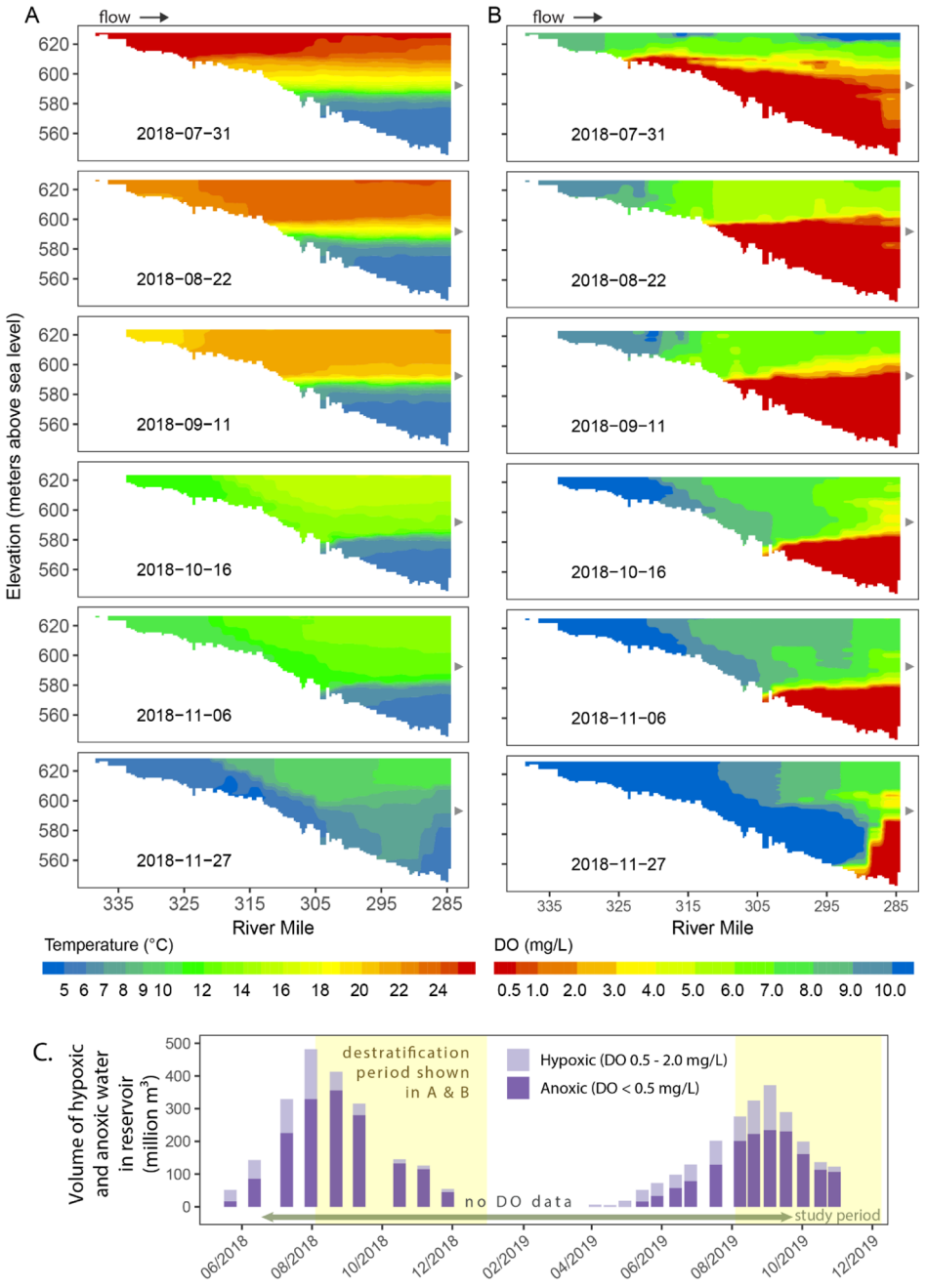


**Figure 1.** Longitudinal cross sections of Brownlee Reservoir (A) water temperature and (B) DO concentrations on different dates during the 2018 destratification period. River flow is from left to right. Gray triangles indicate penstock centerline elevation. A companion set of plots for the 2019 destratification period is provided in Figure S3. (C) Volume of hypoxic and anoxic water in Brownlee Reservoir during late May 2018 to November 2019, with the study period indicated along the *x*-axis [°C, degrees Celsius; $m^3$, cubic meters; mg/L, milligrams per liter].

0.00001 g (all other samples) on a digital balance. The biomass associated with each functional class in the entire sample was calculated based on the proportion of the original sample that was sorted and the volume of water filtered during each deployment based on the flow meter readings. The biological samples were analyzed for MeHg at the USGS Contaminant Ecology Research Laboratory (Corvallis, OR, USA) following EPA method 1630,[28] and the results are reported on a dry weight basis. Additional method details are provided in the Supporting Information, and QAQC results are summarized in Tables S2 and S3.

**Brownlee Reservoir Water Temperature and Dissolved Oxygen.** Vertical profiles of water temperature and dissolved oxygen (DO) were collected in Brownlee Reservoir to monitor the stratification status and to estimate the volume of hypoxic and anoxic water in the reservoir. Vertical profiles were collected using a SeaBird Electronics SeaCat SBE 19-plus system every 3.2 km along the thalweg of Brownlee Reservoir (22 locations) at 2 week intervals between April and late December throughout the study period. In the distances between profiles, water temperature and DO were estimated using the inverse distance interpolation method in Tecplot 360, resulting in a continuous longitudinal water temperature and DO profile of Brownlee Reservoir every 2 weeks. The total reservoir volume of hypoxic (0.5 < DO < 2.0 mg/L) and anoxic (DO < 0.5 mg/L) water corresponding to each profile date was estimated using the


https://doi.org/10.1021/acs.est.2c03958
Environ. Sci. Technol. 2022, 56, 13751−13760

longitudinal DO profiles and reservoir stage and bathymetry data, following the assumption that DO along the thalweg was horizontally uniform.

**Data Analysis.** All data analysis was done using R software.[30] Nonparametric statistical tests were used because the data were non-normally distributed. Spatial, temporal, and matrix comparisons of concentrations were done using either the Wilcoxon rank sum test in the base R package *stats*[30] or the Kruskal–Wallis multiple comparison test in the R package pgirmess.[31] Correlations between different variables (e.g., MeHg concentrations in water and zooplankton) were assessed using the Spearman rank test in the R package Hmisc.[32] To examine the relations between aqueous and biological MeHg, which were each sampled biweekly but not on the same day, the time series of daily aqueous MeHg concentrations were developed using the composite method in the R software package loadflex.[33] The daily mercury loads in aqueous and biological samples were estimated using the composite method[34] in loadflex.[33] The composite method combines regression and interpolation and has been shown to provide more accurate load estimates for a variety of constituents compared to either regression or interpolation alone, especially for high-frequency (i.e., biweekly) datasets.[35] The regression models used in the composite method were developed using LOADEST model nine, which includes continuous predictor variables related to streamflow and season.[36] The mean daily streamflow data used in load estimates were from Idaho Power Company streamgages.[37] Additional details on data analysis are described in the Supporting Information.

## RESULTS AND DISCUSSION

**Brownlee Stratification and Destratification.** A temporal analysis of the Brownlee Reservoir stratification status was conducted using water temperature and DO profiles to aid the interpretation of the MeHg export data. At the beginning of the study in June 2018, Brownlee Reservoir was thermally stratified and anoxic or hypoxic in portions of the transition zone, metalimnion, and throughout the hypolimnion. Destratification began in August (between 7/31/2018 and 8/22/2018) with erosion and mixing of the anoxic and hypoxic water in the transition zone (Figure 1A,B), reducing the total volume of hypoxic and anoxic water in the reservoir (Figure 1C). By early- to mid-October (Figure 1A,B), approximately 65% of anoxic and 90% of hypoxic water volumes present in late July had been eroded and mixed into overlying oxic waters or flushed from the reservoir (Figure 1C), and the remaining hypoxic and anoxic water was limited to the hypolimnion. A second stage of destratification occurred between mid-November and early- to mid-December (Figure 1C). By December 11, the reservoir was well mixed (as indicated by a water temperature gradient of <1.5 °C for all depths between River Miles 305 and 285; DO values not available due to freezing of the sensor) and remained so for the remainder of the winter and early spring. Thus, the 2018 destratification period spanned from August to December, with most of the physical mixing occurring in August to September (mixing of the transition zone and erosion of the metalimnion) and November to December (the turnover of the hypolimnion). In 2019, hypoxic and anoxic water gradually built up from April to the maxima in early September, which then decreased again with the onset of destratification (Figures 1C and S3).

**Masses of Biological Material and SPM in Water.** The biomass density (mass of biological material per cubic meter of water) in the samples at reservoir outflow locations varied considerably across different biological compartments (Figure 2A). Fish and other invertebrates generally had the lowest biomass density. In contrast, the biomass densities of coarse and fine detritus and zooplankton were 1 and 2–3 orders of magnitude greater, respectively, than those of fish. Masses of SPM per volume of water were approximately 2 orders of magnitude greater than those of zooplankton. The biomass densities of coarse and fine detritus and the masses of SPM per volume of water were significantly and positively correlated with the streamflow (Figure S6).

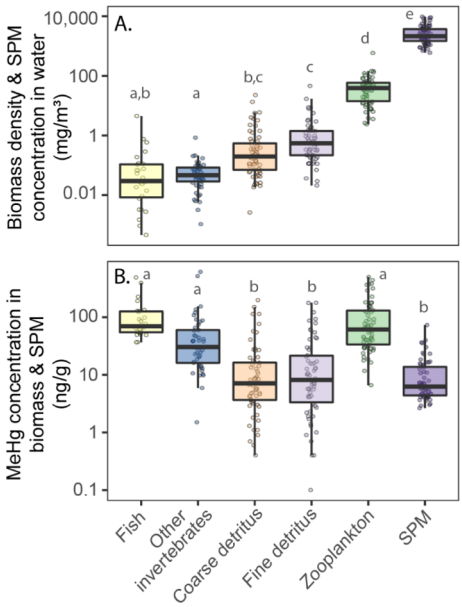


**Figure 2.** (A) Biomass density and SPM in water and (B) MeHg concentration in biological material and SPM in samples from Brownlee Outflow and Oxbow Outflow, June 2018 to September 2019. Boxplots present median and quartile ranges, and whiskers extend 1.5× the interquartile ranges. Lower case letters (a–e) indicate statistical differences between groups based on the Kruskal–Wallis multiple comparison test, with $p$ value of 0.05 [SPM, suspended particulate material; ng/g, nanograms per gram; mg/m$^3$, milligrams per cubic meter].

**MeHg Concentrations in Water.** Aqueous MeHg concentrations ($MeHg_F$, $MeHg_{PV}$, and $MeHg_{PG}$) and the percentages of filter-passing and particulate THg as MeHg (% $MeHg_F$ and % $MeHg_P$) in Brownlee Outflow samples were higher during August to December 2018 than during the months before and after (Figure 3A–E and Table S5). We observed two distinct peaks in aqueous MeHg concentrations during the August to December 2018 period (Figure 3A–E), coinciding with the two stages of destratification of Brownlee Reservoir. Profiles of Brownlee Reservoir DO (Figure 1B) suggest that the first peak in aqueous MeHg (August to September) was associated with the entrainment and downstream export of anoxic water in the transition zone and metalimnion. Previous studies have identified the potential importance of the oxic–anoxic boundary and metalimnion for both methylation and biological uptake of Hg. Eckley and Hintelman[9] reported maximum methylation potentials at the oxic–anoxic boundary in Canadian lakes, with decreasing methylation potentials at greater depths. In Davis Creek Reservoir (California, USA), Slotton et al.[19] reported a dense seasonal lens of photosynthetic anaerobic bacteria in the lower metalimnion immediately below


https://doi.org/10.1021/acs.est.2c03958
Environ. Sci. Technol. 2022, 56, 13751–13760

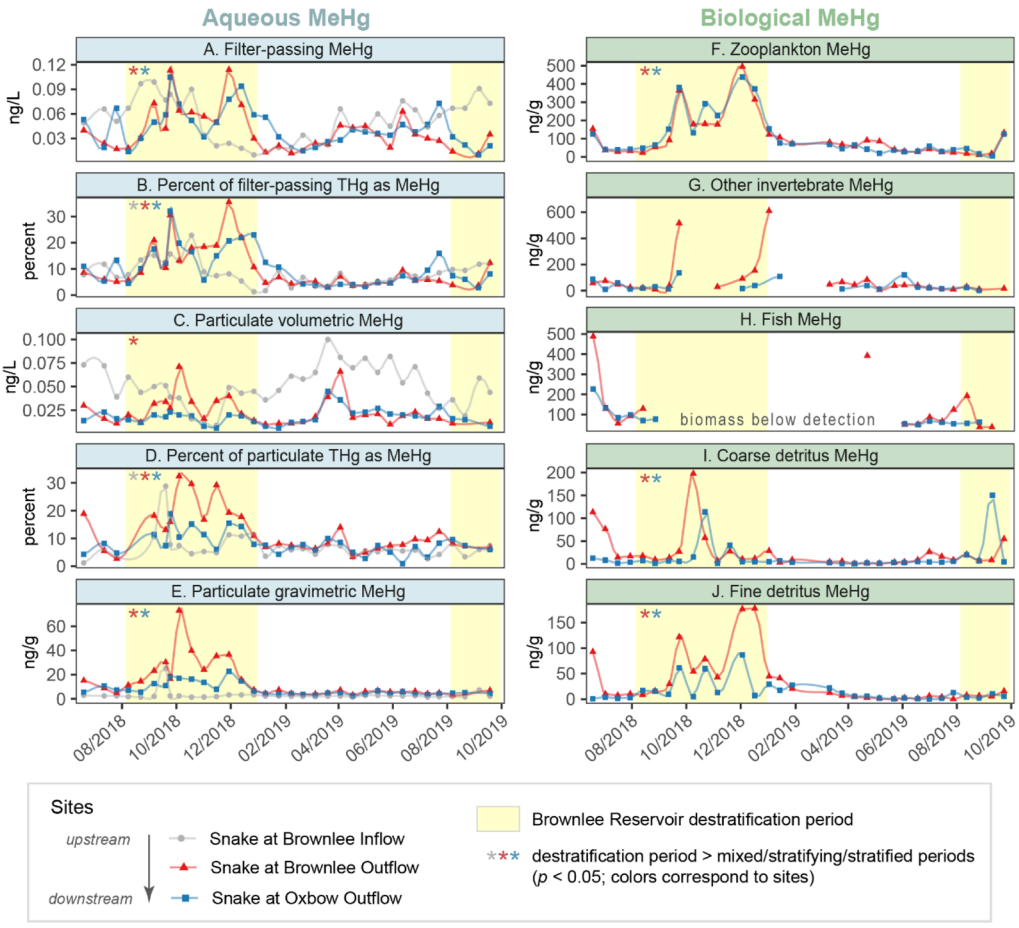


**Figure 3.** Aqueous and biological methylmercury (MeHg) at Brownlee Inflow, Brownlee Outflow, and Oxbow Outflow, June 2018 to September 2019. Data gaps in fish and other invertebrates indicate dates when the biomass was below detection. August through December of each year are highlighted in yellow to indicate the approximate destratification periods of Brownlee Reservoir. Data for the Brownlee Inflow location were only available for plots A–E [THg, total mercury; ng/L, nanograms per liter; ng/g, nanograms per gram dry weight].

the thermocline, and based on the entrainment of this layer into the mixed layer coincident with the increases in THg concentrations in juvenile bass hypothesized that this layer may be a seasonally important source of bioavailable Hg.

Following the increase in aqueous MeHg concentrations at Brownlee Outflow in August to September 2018, concentrations decreased by 56% in October 2018, coincident with the pause in destratification (Figure 1). Concentrations then rebounded in late November 2018 (Figure 3), coincident with the entrainment and downstream export of anoxic water in the hypolimnion (Figure 1B).

Aqueous MeHg concentrations at Oxbow Outflow were similar to ($p > 0.05$; $MeHg_F$ and $MeHg_{PV}$) or less than ($p < 0.05$; $\%MeHg_P$ and $MeHg_{PG}$) those at Brownlee Outflow, but in both cases followed a similar temporal pattern to those at Brownlee Outflow (Figure 3A–E and Table S5). This temporal pattern of increased aqueous MeHg concentrations at Brownlee and Oxbow Outflows during the August to December destratification period has previously been observed during 2015–2017 as well (Figure S7).[17] In contrast, aqueous MeHg at Brownlee Inflow varied independently of this pattern (Figure 3A–E), suggesting that the outflow MeHg concentrations were controlled by in-reservoir, rather than upstream, processes. The importance of in-reservoir processes on MeHg export from Brownlee Reservoir, originally discussed by Baldwin et al.,[17] is further supported by the decoupling of aqueous MeHg concentrations between Brownlee Inflow and Brownlee Outflow from 2014 to 2021, as discussed in the Supporting Information and presented in Figures S7 and S8.

Unlike in 2018, Brownlee Outflow and Oxbow Outflow aqueous MeHg concentrations showed little or no increase through the 2019 destratification period (Figure S7). This coincided with a smaller volume of anoxic + hypoxic water in Brownlee Reservoir in 2019 versus 2018 (Figure S7A). Analysis of aqueous MeHg and DO data from 2014 to 2020 (Figure S7) showed the reservoir anoxic volume to be a good predictor of aqueous MeHg concentrations at Brownlee Outflow during the destratification period ($MeHg_F$ $R^2$ of 0.79, Figure 4; $MeHg_{PV}$ $R^2$ of 0.66). While anoxia is known to be a key factor in MeHg production in the metalimnion and hypolimnion,[9] our results indicate that the volume of reservoir anoxia prior to destratification may be a key driver of MeHg export downstream during destratification. This finding is especially relevant in light of recent global projections of increasing anoxia in reservoirs driven by land use and climate change.[5] A greater understanding of the factors controlling the development and extent of reservoir anoxia and how those factors can be mitigated in the face of land use and climate change will support reservoir management decision-making.

**MeHg Concentrations in Biota.** Among the biological compartments, MeHg concentrations were greatest in fish (36.6–488 ng/g), zooplankton (6.60–495 ng/g), and other


https://doi.org/10.1021/acs.est.2c03958
Environ. Sci. Technol. 2022, 56, 13751–13760

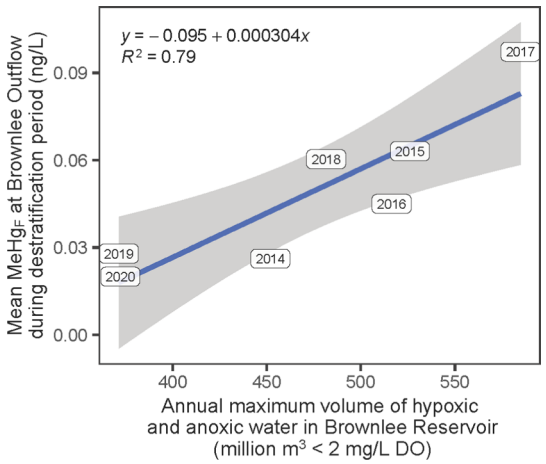


**Figure 4.** Relationship between the annual maximum volume of Brownlee Reservoir hypoxic and anoxic water and concentrations of filter-passing methylmercury ($MeHg_F$) at Brownlee Outflow during the destratification period (August to December) [ng/L, nanograms per liter; mg/L, milligrams per liter; $m^3$, cubic meters; DO, dissolved oxygen].

invertebrates (1.50−610 ng/g) (Figure 2B and Table S5). In contrast, MeHg concentrations in coarse and fine detritus were generally the lowest (0.10−198 ng/g) and were comparable to those of SPM. The temporal pattern of MeHg in zooplankton and both detritus categories at Brownlee Outflow followed that of aqueous MeHg, indicating the rapid uptake (zooplankton) and partitioning (detritus) of MeHg concurrent with the reservoir destratification (Figure 3F−J and Table S5). MeHg of invertebrates in the Brownlee Outflow samples followed the same approximate pattern as that of zooplankton and detritus, but the data gaps prevent the determination of the exact timing of those maxima (Figure 3G). Temporal patterns in fish MeHg concentrations were not discernible because fish were predominately associated with a high flow at the reservoir outflow locations and were absent from the samples throughout much of the study period (Figure 3H).

As was observed with aqueous MeHg concentrations, biological MeHg concentrations appeared to be lower during the 2019 destratification period than during the 2018 destratification period, although biological sampling concluded prior to complete destratification (Figure 3). Zooplankton, invertebrate, and fish MeHg concentrations at Oxbow Outflow were similar ($p > 0.05$) to those at Brownlee Outflow, whereas detrital concentrations were slightly lower ($p < 0.05$). In both cases, biological MeHg concentrations at Oxbow Outflow followed a similar temporal pattern, as observed at Brownlee Outflow.

We evaluated the linkages between aqueous MeHg concentrations and biological MeHg concentrations at each location using Spearman correlations (Table S6). Across all sampling events, regardless of reservoir stratification, zooplankton MeHg concentrations were significantly correlated with $MeHg_F$ at both Brownlee Outflow ($r = 0.70$, $p < 0.0001$) and Oxbow Outflow ($r = 0.49$, $p = 0.0049$) (Figure 5A). However, when data were binned by the Brownlee Reservoir stratification status (i.e., mixed, stratifying and stratified, destratifying), we found that the relationship was only significant during the destratifying period (Brownlee Outflow: $r = 0.92$, $p < 0.0001$; Oxbow Outflow: $r = 0.91$, $p < 0.0001$; Figure 5B−D). This suggests that the destratification period is a critical time for MeHg formed in the metalimnion and hypolimnion to become incorporated at the base of the aquatic food web. Zooplankton MeHg concentrations were also correlated with $MeHg_{PG}$ at both sites, although the relationships were not as strong as with $MeHg_F$ (Table S6). Neither fish nor invertebrate MeHg concentrations were significantly correlated with $MeHg_F$ (Table S6). While this could be related to gaps in our fish and other invertebrate data, a similar lack of correlation has been observed elsewhere[20] and is likely attributed to a combination of food web complexity and spatial/temporal scale differences for MeHg incorporation among the different biological matrices. Fish MeHg was weakly correlated with zooplankton MeHg at Brownlee Outflow ($r = 0.49$, $p = 0.078$) and more strongly correlated with Oxbow Outflow ($r = 0.56$, $p = 0.046$) (Table S6), supporting the idea that plankton MeHg is an important determinant of MeHg in fish within the reservoirs.[20,38,39]

A limited number of studies have reported the rapid increase in MeHg concentrations on SPM and in biota concurrent with the reservoir destratification that we observed in this study.

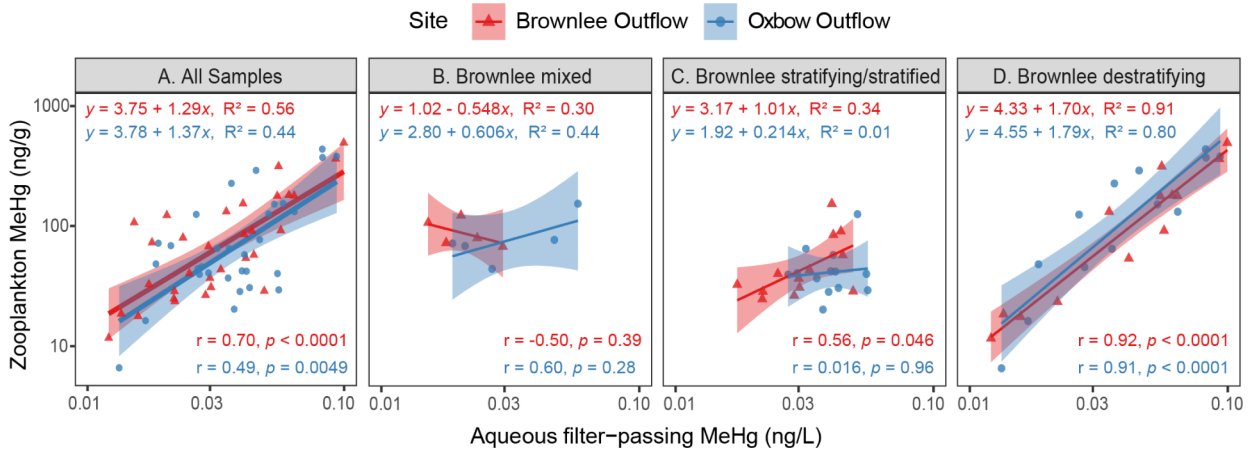


**Figure 5.** Relationship between methylmercury (MeHg) in filter-passing water and zooplankton samples from Brownlee Outflow and Oxbow Outflow. (A) Samples from the entire study period June 2018 to September 2019; (B−D) samples binned based on the stratification state of Brownlee Reservoir. Linear regressions are shown as solid lines, and confidence intervals of the fit are shaded [ng/L, nanograms per liter; ng/g, nanograms per gram dry weight; $r$ = Spearman correlation; $p$ = $p$ value on the Spearman correlation].



https://doi.org/10.1021/acs.est.2c03958
Environ. Sci. Technol. 2022, 56, 13751−13760

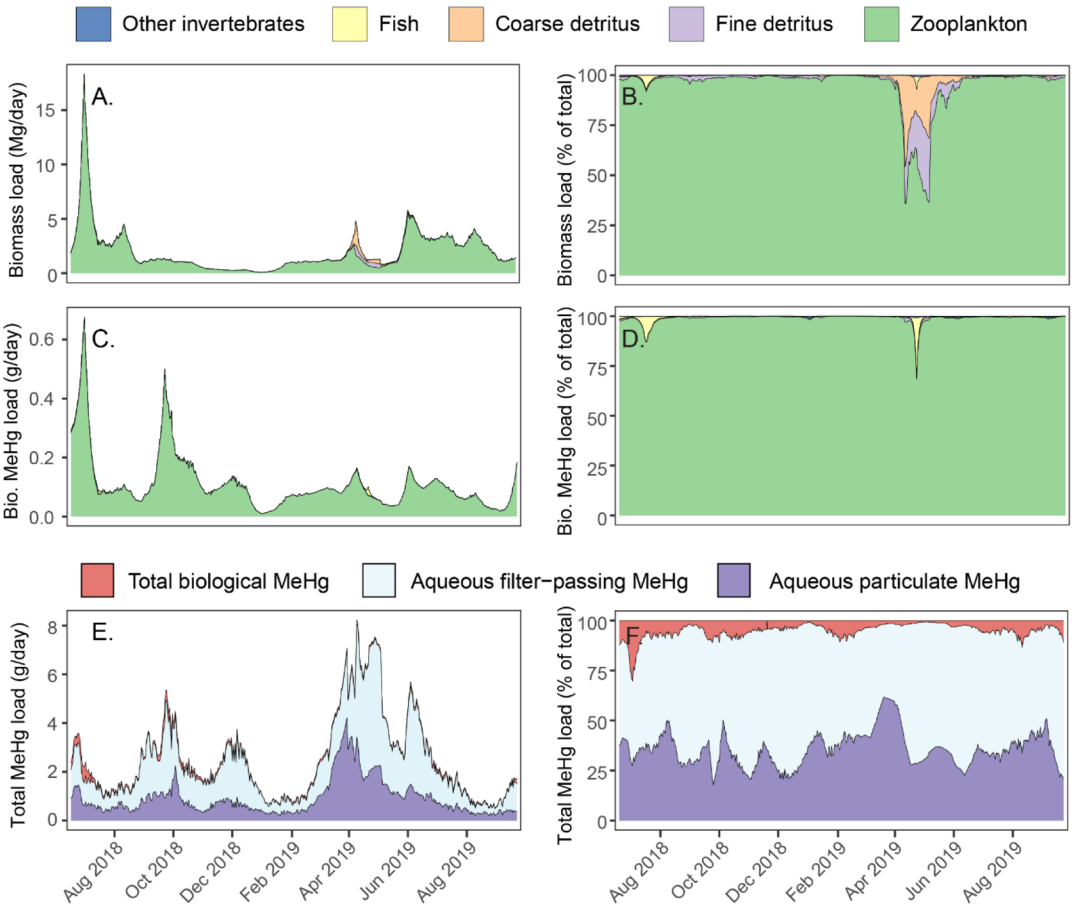


**Figure 6.** Brownlee Outflow (A,B) biomass and (C,D) biological (bio) methylmercury (MeHg) loads in individual biological compartments, and (E,F) total biological MeHg load compared with aqueous (filter-passing and particulate) MeHg loads. Load estimates based on biweekly samples, June 2018 to September 2019. A companion figure for Oxbow Outflow is provided in Figure S13 [Mg, megagrams; g, grams].

Herrin et al.[11] reported rapid increases in particle-associated and Daphnia MeHg, concurrent with the thermal destratification and mixing of anoxic hypolimnetic water in Devils Lake, Wisconsin (USA); they concluded that much of the mass of MeHg built up in the hypolimnion was rapidly taken up by particulate matter in the mixed zone during turnover. Similarly, Slotton et al.[19] reported rapid increases in THg (MeHg was not analyzed) in zooplankton and juvenile fish, concurrent with the thermal destratification and mixing of anoxic hypolimnetic water in Davis Creek Reservoir. Whereas Herrin et al. and Slotton et al. focused on in-lake and in-reservoir processes, the current study fills an important knowledge gap by showing with the high temporal resolution that these processes also influence downstream MeHg export from reservoirs.

**MeHg Loads.** Daily loads were estimated for (1) biomasses (zooplankton, other invertebrates, fish, and fine and coarse detritus), (2) SPM, (3) biological MeHg, and (4) aqueous MeHg ($MeHg_F$ and $MeHg_{PV}$) at Brownlee Outflow and Oxbow Outflow. Here, we present load estimates for the June 2018 to September 2019 study period. For comparison over a wider range of hydrological conditions, the annual load estimates of aqueous MeHg and inorganic divalent Hg for the period 2015−2020 are provided in Figures S9 and 10 and Table S7.

Daily loads of total biomass ranged from 0.0735 to 18.3 megagrams/day (Mg/day; mean 2.04 Mg/day) at Brownlee Outflow and 0.0907 to 17.5 Mg/day (mean 1.75 Mg/day) at Oxbow Outflow (Figures 6A and S13A and Table S8). At both locations, the biomass loads were greater in spring and summer months, when streamflows were the greatest, compared to fall and winter. Zooplankton dominated biomass loads at both locations, comprising, on average, 94.8 and 88.2% of the total biomass loads at Brownlee Outflow at Oxbow Outflow, respectively (Figures 6B and S13B and Table S8). Coarse and fine detritus together comprised 4.91 and 11.7%, respectively, of the total biomass loads at the two locations. The export of detritus biomass was primarily observed during the March to June (2019) spring snowmelt period, during which they made up half or more of the total biomass loads (Figures 6B and S13B). Fish made up only 0.190 and 0.034% of the total biomass load at Brownlee Outflow and Oxbow Outflow, respectively. Similarly, other invertebrates made up only 0.150 and 0.070% of the total biomass load at Brownlee Outflow and Oxbow Outflow, respectively. The loads of SPM exceeded the loads of biomass by several orders of magnitude, ranging from 14,800 to 943,000 Mg/day (mean 144,000 Mg/day) at Brownlee Outflow and 14,200 to 1,330,000 Mg/day (mean 182,000 Mg/day) at Oxbow Outflow (Table S8).

The total biological MeHg loads ranged from 0.00906 to 0.677 g/day (mean 0.111 g/day) at Brownlee Outflow and 0.00674 to 0.345 g/day (mean 0.0945 g/day) at Oxbow Outflow (Figures 6C and S13C and Table S9). Biological MeHg loads were almost entirely associated with zooplankton, which accounted for 98.9 and 96.7% of the total biological MeHg load at each location, on average (Figures 6D and S13D and Table S9). The second greatest share of the total biological MeHg load was fish at Brownlee Outflow (mean 0.584%) and


https://doi.org/10.1021/acs.est.2c03958
Environ. Sci. Technol. 2022, 56, 13751−13760

fine detritus at Oxbow Outflow (2.66%). At both locations, some of the highest biological MeHg loads were in September 2018 (Figures 6C and S13C), a period when the biomass loads were relatively low (Figures 6A and S13A) but biological MeHg concentrations were high (Figure 3), coincident with the first stage of destratification of Brownlee Reservoir (Figure 1).

The total biological MeHg loads were far surpassed by the loads of $MeHg_P$ and $MeHg_F$ (Figures 6E and S13E). Loads of $MeHg_P$ were nearly an order of magnitude greater than the total biological MeHg loads, ranging between 0.197 and 4.22 g/day (mean 0.912 g/day) at Brownlee Outflow and 0.0643−3.24 g/day (mean 0.814 g/day) at Oxbow Outflow (Table S9). The greatest $MeHg_P$ loads occurred during the spring snowmelt period, when streamflows were the greatest, despite low MeHg concentrations in particles during that time (Figure 3E). $MeHg_F$ loads ranged between 0.270 and 5.24 g/day (mean 1.53 g/day) at Brownlee Outflow and 0.172−4.64 g/day (mean 1.60 g/day) at Oxbow Outflow (Table S9). The combined aqueous ($MeHg_F$ and $MeHg_P$) plus biological MeHg load at Brownlee Outflow averaged 2.55 g/day and comprised 5.22% biological, 59.1% $MeHg_F$, and 35.7% $MeHg_P$ (Figure 6E,F and Table S9). The combined aqueous plus biological MeHg load at Oxbow Outflow was similar, averaging 2.51 g/day, and comprised 4.88% biological, 65.0% $MeHg_F$, and 30.1% $MeHg_P$ (Figure S13E,F and Table S9).

The relative distribution of MeHg export among individual aqueous and biological compartments in the current study is consistent with the previous findings from Caniapiscau Reservoir (Quebec, Canada).[21] In Brownlee Reservoir, the distribution was 59.1% $MeHg_F$, 35.7% $MeHg_P$, 5.17% zooplankton, 0.03% fish, <0.01% other invertebrates, and 0.016% detritus. In Caniapiscau Reservoir, the distribution was 64.3% $MeHg_F$, 33.2% $MeHg_P$, 1.54% zooplankton, 0.85% phytoplankton, 0.1% fish, <0.01% other invertebrates, and 0.01% detritus.[21] The relatively small proportion of biological MeHg export (4.87−5.22% of the total MeHg export; Table S9) relative to particle-bound MeHg export (30.1−35.7%) in the current study reflects the quantity of biomass versus suspended particles in the water column. MeHg concentrations in zooplankton, which made up the vast majority of the total biomass (Figure 6B), were 10× greater than MeHg concentrations on suspended particles (Figure 2B), but suspended particles were 100× more abundant (Figure 2A). The suspended particles likely included some phytoplankton and zooplankton, in addition to mineral particles, but in relatively minor proportions: SPM data from Brownlee and Oxbow Outflows averaged approximately 11% particulate organic carbon,[24] indicating that the majority of SPM was mineral. We did not directly sample phytoplankton and zooplankton <125 $\mu$m, but, based on the small proportion of particulate organic carbon in SPM samples, we expect MeHg loads associated with phytoplankton and zooplankton <125 $\mu$m to be small. In Caniapiscau Reservoir, phytoplankton accounted for <1% of the total MeHg export.[21]

Although our results show that the percentage of total MeHg export from the reservoirs as biological MeHg was small compared to that of the aqueous compartments, we anticipate that the biological MeHg disproportionately impacts MeHg concentrations in biota downstream of the dams because fish are primarily exposed to MeHg through their diet.[40] Thus, understanding the processes driving MeHg production within reservoirs and MeHg uptake at the base of the food web during and after destratification is critical to managing mercury in fish within and downstream of reservoirs.

## ■ ASSOCIATED CONTENT

### Supporting Information

The Supporting Information is available free of charge at https://pubs.acs.org/doi/10.1021/acs.est.2c03958.

All data collected as part of this study are publicly available online.[24,25] Additional information on the study area, data collection and analysis, and QAQC and environmental sample result summaries (including concentrations and loads for an expanded period from 2014 to 2021 and at two additional sites) are provided in the supporting information (PDF).

Supporting information tables include: Summary of relative percent differences between concentrations in duplicate water samples; relative standard deviation and standard error among replicate biomass measurements for zooplankton, other invertebrates, fish, coarse detritus, and fine detritus samples; quality assurance−quality control results for the analysis of methylmercury in biological materials; regression equations used to estimate methylmercury concentrations in fish and other invertebrates based on MeHg concentrations in zooplankton; summary of methylmercury concentrations in water and biological samples from Brownlee Inflow, Brownlee Outflow, and Oxbow Outflow, June 2018−September 2019; Spearman correlation coefficients between mercury concentrations in individual aqueous and biological compartments; and estimated mean daily loads of inorganic and methylmercury fractions and suspended particulate material in water samples from the reservoir inflow and outflow locations, 2015−2020 (XLSX)

## ■ AUTHOR INFORMATION


### Corresponding Author

**Austin K. Baldwin** − *U.S. Geological Survey, Idaho Water Science Center, Boise, Idaho 83702, United States;* orcid.org/0000-0002-6027-3823; Phone: (208) 387-1365; Email: akbaldwi@usgs.gov

### Authors

**Collin A. Eagles-Smith** − *U.S. Geological Survey, Forest and Rangeland Ecosystem Science Center, Corvallis, Oregon 97330, United States;* orcid.org/0000-0003-1329-5285

**James J. Willacker** − *U.S. Geological Survey, Forest and Rangeland Ecosystem Science Center, Corvallis, Oregon 97330, United States;* orcid.org/0000-0002-6286-5224

**Brett A. Poulin** − *Department of Environmental Toxicology, University of California at Davis, Davis, California 95616, United States;* orcid.org/0000-0002-5555-7733

**David P. Krabbenhoft** − *U.S. Geological Survey, Upper Midwest Water Science Center, Madison, Wisconsin 53726, United States;* orcid.org/0000-0003-1964-5020

**Jesse Naymik** − *Idaho Power Company, Boise, Idaho 83702, United States*

**Michael T. Tate** − *U.S. Geological Survey, Upper Midwest Water Science Center, Madison, Wisconsin 53726, United States*

**Dain Bates** − *Idaho Power Company, Boise, Idaho 83702, United States*

**Nick Gastelecutto** − *Idaho Power Company, Boise, Idaho 83702, United States*
**Charles Hoovestol** − *Idaho Power Company, Boise, Idaho 83702, United States*
**Chris Larsen** − *Idaho Power Company, Boise, Idaho 83702, United States*
**Alysa M. Yoder** − *U.S. Geological Survey, Idaho Water Science Center, Boise, Idaho 83702, United States;* orcid.org/0000-0002-3683-6729
**James Chandler** − *Idaho Power Company, Boise, Idaho 83702, United States*
**Ralph Myers** − *Idaho Power Company, Boise, Idaho 83702, United States*

Complete contact information is available at: https://pubs.acs.org/10.1021/acs.est.2c03958

### Notes

The authors declare no competing financial interest.

## ■ ACKNOWLEDGMENTS

The authors gratefully acknowledge M. McLeod and T. Richter at Idaho Power Company and T. Glidden, J. Pierce, C. Rumrill, B. Johnson, J. DeWild, S. Janssen, and J. Ogorek, at the U.S. Geological Survey (USGS), for sample collection and analysis. M. Marvin-DiPasquale and R. Harris made valuable contributions to study planning, data interpretation, and discussions. Funding and support were provided by Idaho Power Company, the Idaho Department of Environmental Quality, and the USGS Cooperative Funding, Toxics Substances Hydrology, and Contaminant Biology programs (Ecosystems Mission Area). Any use of trade, firm, or product names is for descriptive purposes only and does not imply endorsement by the U.S. Government.

## ■ REFERENCES

(1) Louis, St. V.; Kelly, C. A.; Duchemin, É.; Rudd, J. W. M.; Rosenberg, D. M. Reservoir Surfaces as Sources of Greenhouse Gases to the Atmosphere: A Global Estimate: Reservoirs Are Sources of Greenhouse Gases to the Atmosphere, and Their Surface Areas Have Increased to the Point Where They Should Be Included in Global Inventories of Anthropogenic Emissions of Greenhouse Gases. *BioScience* **2000**, *50*, 766−775.
(2) Zarfl, C.; Lumsdon, A. E.; Berlekamp, J.; Tydecks, L.; Tockner, K. A Global Boom in Hydropower Dam Construction. *Aquat Sci* **2015**, *77*, 161−170.
(3) Bohada-Murillo, M.; Castaño-Villa, G. J.; Fontúrbel, F. E. Effects of Dams on Vertebrate Diversity: A Global Analysis. *Diversity* **2021**, *13*, 528.
(4) Ekka, A.; Pande, S.; Jiang, Y.; der Zaag, P. Anthropogenic Modifications and River Ecosystem Services: A Landscape Perspective. *Water (Switz.))* **2020**, *12*, 2706.
(5) Jane, S. F.; Hansen, G. J. A.; Kraemer, B. M.; Leavitt, P. R.; Mincer, J. L.; North, R. L.; Pilla, R. M.; Stetler, J. T.; Williamson, C. E.; Woolway, R. I.; Arvola, L.; Chandra, S.; DeGasperi, C. L.; Diemer, L.; Dunalska, J.; Erina, O.; Flaim, G.; Grossart, H.-P.; Hambright, K. D.; Hein, C.; Hejzlar, J.; Janus, L. L.; Jenny, J.-P.; Jones, J. R.; Knoll, L. B.; Leoni, B.; Mackay, E.; Matsuzaki, S.-I. S.; McBride, C.; Müller-Navarra, D. C.; Paterson, A. M.; Pierson, D.; Rogora, M.; Rusak, J. A.; Sadro, S.; Saulnier-Talbot, E.; Schmid, M.; Sommaruga, R.; Thiery, W.; Verburg, P.; Weathers, K. C.; Weyhenmeyer, G. A.; Yokota, K.; Rose, K. C. Widespread Deoxygenation of Temperate Lakes. *Nature* **2021**, *594*, 66−70.
(6) Morales-Marin, L. A.; Carr, M.; Sadeghian, A.; Lindenschmidt, K. E. Climate Change Effects on the Thermal Stratification of Lake Diefenbaker, a Large Multi-Purpose Reservoir. *Can. Water Resour. J.* **2021**, *46*, 1−16.
(7) Lee, R. M.; Biggs, T. W. Impacts of Land Use, Climate Variability, and Management on Thermal Structure, Anoxia, and Transparency in Hypereutrophic Urban Water Supply Reservoirs. *Hydrobiologia* **2015**, *745*, 263−284.
(8) Marcé, R.; Moreno-Ostos, E.; López, P.; Armengol, J. The Role of Allochthonous Inputs of Dissolved Organic Carbon on the Hypolimnetic Oxygen Content of Reservoirs. *Ecosystems* **2008**, *11*, 1035−1053.
(9) Eckley, C. S.; Hintelmann, H. Determination of Mercury Methylation Potentials in the Water Column of Lakes across Canada. *Sci. Total Environ.* **2006**, *368*, 111−125.
(10) Canavan, C. M.; Caldwell, C. A.; Bloom, N. S. Discharge of Methylmercury-Enriched Hypolimnetic Water from a Stratified Reservoir. *Sci. Total Environ.* **2000**, *260*, 159−70.
(11) Herrin, R. T.; Lathrop, R. C.; Gorski, P. R.; Andren, A. W. Hypolimnetic Methylmercury and Its Uptake by Plankton during Fall Destratification: A Key Entry Point of Mercury into Lake Food Chains? *Limnol. Oceanogr.* **1998**, *43*, 1476−1486.
(12) Watras, C. J.; Back, R. C.; Halvorsen, S.; Hudson, R. J.; Morrison, K. A.; Wente, S. P. Bioaccumulation of Mercury in Pelagic Freshwater Food Webs. *Sci. Total Environ.* **1998**, *219*, 183−208.
(13) Wentz, D. A.; Brigham, M. E.; Chasar, L. C.; Lutz, M. A.; Krabbenhoft, D. P. *Mercury in the Nation's Streams—Levels, Trends, and Implications*; U.S. Geological Survey Circular, 2014; p 139590.
(14) Choi, A. L.; Grandjean, P.; Choi, A. L.; Grandjean, P. Methylmercury Exposure and Health Effects in Humans. *Environ. Chem.* **2008**, *5*, 112−120.
(15) Crump, K. L.; Trudeau, V. L. Mercury-Induced Reproductive Impairment in Fish. *Environ. Toxicol. Chem.* **2009**, *28*, 895−907.
(16) Tan, S. W.; Meiller, J. C.; Mahaffey, K. R. The Endocrine Effects of Mercury in Humans and Wildlife. *Crit. Rev. Toxicol.* **2009**, *39*, 228−269.
(17) Baldwin, A. K.; Poulin, B. A.; Naymik, J.; Hoovestol, C.; Clark, G. M.; Krabbenhoft, D. P. Seasonal Dynamics and Interannual Variability in Mercury Concentrations and Loads through a Three-Reservoir Complex. *Environ. Sci. Technol.* **2020**, *54*, 9305−9314.
(18) Kasper, D.; Forsberg, B. R.; Amaral, J. H. F.; Leitão, R. P.; Py-Daniel, S. S.; Bastos, W. R.; Malm, O. Reservoir Stratification Affects Methylmercury Levels in River Water, Plankton, and Fish Downstream from Balbina Hydroelectric Dam, Amazonas, Brazil. *Environ. Sci. Technol.* **2014**, *48*, 1032−1040.
(19) Slotton, D. G.; Reuter, J. E.; Goldman, C. R. Mercury Uptake Patterns of Biota in a Seasonally Anoxic Northern California Reservoir. *Water, Air, Soil Pollut.* **1995**, *80*, 841−850.
(20) Chen, C. Y.; Stemberger, R. S.; Klaue, B.; Blum, J. D.; Pickhardt, P. C.; Folt, C. L. Accumulation of Heavy Metals in Food Web Components across a Gradient of Lakes. *Limnol. Oceanogr.* **2000**, *45*, 1525−1536.
(21) Schetagne, R.; Doyo, J. F.; Fournier, J. J. Export of Mercury Downstream from Reservoirs. *Sci. Total Environ.* **2000**, *260*, 135−45.
(22) Myers, R.; Harrison, J.; Parkinson, S. K.; Hoelscher, B.; Naymik, J.; Parkinson, S. E. *Pollutant Transport and Processing in the Hells Canyon Complex; Technical Report Appendix E.2.2-2*; Idaho Power Company, 2003, p 202.
(23) Clark, G. M.; Naymik, J.; Krabbenhoft, D. P.; Eagles-Smith, C. A.; Aiken, G. R.; Marvin-DiPasquale, M. C.; Harris, R. C.; Myers, R. *Mercury Cycling in the Hells Canyon Complex of the Snake River, Idaho and Oregon*; USGS, Fact Sheet, 2016−3051.
(24) Poulin, B. A.; Breitmeyer, S. E.; Krabbenhoft, D. P.; Tate, M. T.; DeWild, J. F.; Ogorek, J. M.; Babiarz, C. L.; Janssen, S. E.; Marvin-DiPasquale, M. C.; Agee, J. L.; Kakouros, E.; Kieu, L.; Arias, M.; Conaway, C.; Antweiler, R. C.; Baldwin, A. K.; Yoder, A.; Clark, G. M.; Aiken, G. R. *Chemical Characterization of Water and Suspended Sediment of the Snake River and Hells Canyon Complex (Idaho, Oregon)*; U.S. Geological Survey Data Release, 2020.
(25) Baldwin, A. K.; Willacker, J. J.; Eagles-Smith, C.; Bates, D. *Biomass and Methylmercury Concentrations in Biweekly Biological*

*Samples from Brownlee and Oxbow Reservoir Outflows, Snake River Hells Canyon Complex (Idaho-Oregon), 2018−2019*; U.S. Geological Survey Data Release, 2022.
(26) U.S. Environmental Protection Agency. *Method 1631, Revision E: Mercury in Water by Oxidation, Purge and Trap, and Cold Vapor Atomic Fluorescence Spectrometry*, 2002.
(27) Olund, S. D.; DeWild, J. F.; Olson, M. L.; Tate, M. T. Methods for the Preparation and Analysis of Solids and Suspended Solids for Total Mercury. *Techniques and Methods*; USGS, 2004.
(28) U.S. Environmental Protection Agency. *Method 1630: Methyl Mercury in Water by Distillation, Aqueous Ethylation, Purge and Trap, and Cold Vapor Atomic Fluorescence Spectrometry*, 1998.
(29) De Wild, J. F.; Olsen, M. L.; Olund, S. D. Determination of Methyl Mercury by Aqueous Phase Ethylation, Followed by Gas Chromatographic Separation with Cold Vapor Atomic Fluorescence Detection. *USGS Open File Rep.* **2002**, *19*, 445.
(30) R Core Team. *R: A Language and Environment for Statistical Computing*, 2017.
(31) Giraudoux, P. P. *Data Analysis in Ecology. R Package*, Version 1.6.3, 2015.
(32) Harrell, F. E., Jr.; Dupont, C. *Hmisc: Harrell Miscellaneous. R Package*, 2020. Version 4.4-1.
(33) Appling, A. P.; Leon, M. C.; McDowell, W. H. Reducing Bias and Quantifying Uncertainty in Watershed Flux Estimates: The R Package Loadflex. *Ecosphere* **2015**, *6*, 1−25.
(34) Aulenbach, B. T.; Hooper, R. P. The Composite Method: An Improved Method for Stream-Water Solute Load Estimation. *Hydrol. Processes* **2006**, *20*, 3029−3047.
(35) Lee, C. J.; Hirsch, R. M.; Crawford, C. G. *An evaluation of methods for computing annual water-quality loads*; U.S. Geological Survey: Reston, VA, 2019; Vol. *2019−5084*, p 74.USGS Numbered Series 2019−5084.
(36) Runkel, R. L.; Crawford, C. G.; Cohn, T. A. Load Estimator (LOADEST): A FORTRAN Program for Estimating Constituent Loads in Streams and Rivers. *USGS Tech. Methods* **2004**, *4*, A5.
(37) Idaho Power Company. Idaho Power River Flow and Reservoir Information. https://www.idahopower.com/community-recreation/recreation/water-information/stream-flow-data/ (accessed April 08, 2022).
(38) Stewart, A. R.; Saiki, M. K.; Kuwabara, J. S.; Alpers, C. N.; Marvin-DiPasquale, M.; Krabbenhoft, D. P. Influence of Plankton Mercury Dynamics and Trophic Pathways on Mercury Concentrations of Top Predator Fish of a Mining-Impacted Reservoir. *Can. J. Fish. Aquat. Sci.* **2008**, *65*, 2351−2366.
(39) Ward, D. M.; Mayes, B.; Sturup, S.; Folt, C. L.; Chen, C. Y. Assessing Element-Specific Patterns of Bioaccumulation across New England Lakes. *Sci. Total Environ.* **2012**, *421-422*, 230−237.
(40) Hall, B. D.; Bodaly, R. A.; Fudge, R. J. P.; Rudd, J. W. M.; Rosenberg, D. M. Food as the Dominant Pathway of Methylmercury Uptake by Fish. *Water, Air, Soil Pollut.* **1997**, *100*, 13−24.


https://doi.org/10.1021/acs.est.2c03958
*Environ. Sci. Technol.* 2022, 56, 13751−13760